Gas Retention and Release from Nuclear Legacy Waste – 16449

Michael Johnson *, Jeff Peakall *, Michael Fairweather *, Simon Biggs *, **, David Harbottle *, Timothy Hunter *,

* University of Leeds

** University of Queensland

ABSTRACT

The retention of gas within corroded magnox sludge waste at Sellafield, UK and secondary reprocessing waste at Hanford, USA has significant economic and safety implications for decommissioning various nuclear legacy buildings, including the magnox swarf storage silos and first generation magnox storage pond. A series of laboratory scale gas retention tests within magnesium hydroxide soft sediments have revealed a 4-51 Pa yield stress range where consolidated beds could retain sufficient gas to become buoyant with respect to a water supernatant. Density inversion could lead to a Rayleigh-Taylor style instability which could result in an upward transfer of radioactive material from the consolidated bed. The applicable yield stress range suggests that such *rollover events* may occur in weaker sediment than previously hypothesized, based on current understanding of the *fluidization* and *stable channel* mechanisms for gas release from weak and very strong sediments respectively. X-ray computed tomography images of gas retained by 7 Pa yield stress soft sediment reveal both a stable foam layer at the top of the bed and regions dense with microbubbles which could provide pathways for gas transport through the bed. Extension of these pathways, hidden below the surface of the sediment, to the container walls and the foam layer could represent a novel mechanism for gas release from intermediate strength sediments of <100 Pa yield stress.

INTRODUCTION

Decommissioning of the magnox swarf storage silos (MSSS) and first generation magnox storage pond are priority activities for the Sellafield nuclear decommissioning site [1], accounting for a quarter of its annual budget. Long term underwater storage of magnox clad fuel since the 1960s has allowed the magnesium/aluminum cladding alloy to corrode, with precipitation products consolidating into a legacy of corroded magnox sludge waste [2, 3]. Concerns have arisen regarding the periodic release of significant volumes of gas, formed by a combination of corrosion reactions and by radiolysis of the pond and silo liquors, from these consolidated beds.

The potential for periodic gas release has previously been researched in relation to secondary reprocessing wastes stored in underground tanks at the nuclear site in Hanford, Washington [4, 5]. Fluctuations in waste level observed in response to changes in barometric pressure indicate the presence of a significant voidage of trapped gas in the settled bed. Spikes in the concentration of hydrogen, nitrous oxide and ammonia in the tank ullage, coinciding with upward transfer of decay heat from the consolidated bed to the supernatant layer, imply the periodic release of gas through buoyant gas release events (GREs), or *rollover* events.

Retention of gas in soft sediments has provoked interest outside of the nuclear industry, particularly among environmental scientists interested in methane trapped in marine sea beds [6,7], lake bottoms [8] and highly viscous volcanic melts [9]. However, the mechanics of soft sediments during bubble growth and release is not currently well understood and no rheological model is widely accepted [6]. The economic impact of *waste swell* due to gas retention on the transportation and storage of nuclear legacy waste, combined with the need to mitigate risks associated with GREs, add to the already significant incentives to understand gas retention and release from soft sediments.

This study introduces a laboratory scale methodology for investigating bed swell and gas release from soft sediments of a magnesium hydroxide test material. These tests reveal the maximum capacity for gas retention of sediments across a broad range of shear yield stress conditions. These tests are supported with shear yield stress characterization using the vane method and x-ray computed tomography (CT) imaging of bubbles retained within a relatively weak, 7 Pa yield stress soft sediment. The shape characteristics of retained bubbles reveal how the sediment responds to the stress imparted by the growing bubble, while large artefacts in the bed could imply the likely mechanism for gas release from the bed.

THEORY

The capacity of soft sediments to retain substantial volumes of gas is limited by the mechanisms available for gas to be released from the bed. In order for a bubble to be held motionless within the bed, the buoyant force of the bubble, F_b, driven by the difference between the gas free bulk sediment density, ρ_s, and the gas density, ρ_g, must be overcome. The buoyant force of the bubble is given by Eq. (1):

$$\boldsymbol{F_b = \frac{\pi}{6}(\rho_s - \rho_g) g {d_b}^3} \tag{1}$$

For a bubble to remain static, this buoyant force must be in equilibrium with a restraining force imparted by the strength of the sediment network [10]. The shear yield stress, τ, is frequently used as a measure of the strength of soft sediments due to its relative ease of characterization using the vane method [11]. The critical restraining force, F_c, to prevent upward bubble motion is said to be proportional to this shear yield stress and the bubble area:

$$\boldsymbol{F_c \propto \frac{\pi}{4} {d_b}^2 \tau} \tag{2}$$

Since the buoyant force increases with bubble volume, while the critical restraining force increases in proportion to bubble area, the bubble can achieve buoyancy once it grows to a critical diameter, which increases in proportion to the yield stress. Consequently, very weak sediments can only overcome the buoyant motion of very small bubbles. This weak sediment release mechanism will be referred to as *fluidization* and the critical bubble diameter for fluidization is governed by Eq. (3):

$$d_b > k \frac{\tau}{(\rho_s - \rho_g) g} \qquad (3)$$

where k is a dimensionless, material dependent proportionality constant typically less than 25 [10]. Fluidization of the bed by the largest retained bubbles is in turn likely to liberate a *cascade* of smaller bubbles in the pathway and wake of the buoyant bubble [12].

Bubbles in soft sediments very quickly grow to the dimensions of capillaries in the bed, at which point the bubble can expand the cavity and grow spherically, fracture the sediment matrix and form tensile cracks, or displace water from the capillary network and grow as a dendritic bubble [5,6]. The energetics of *capillary invasion* are highly unfavorable in fine-grained cohesive sediments with small capillary dimensions due to the extreme Laplace pressure. The excess bubble pressure, ΔP, given by the difference in pressure between the bubble and the bulk sediment, required for *cavity expansion* increases in proportion to the yield stress of the sediment [8]:

$$\Delta P > \frac{4}{3} \tau \left(1 + ln \left|\frac{G}{\tau}\right|\right) \qquad (4)$$

where G is the shear modulus of the soft sediment.

As a consequence of Eq. 4, the resistance to bubble growth by cavity expansion in high yield stress sediments is substantial and bubbles are forced to break the cohesive and adhesive bonds in the sediment by *tensile fracture*. The merging of cracks formed by tensile fracture with drainage channels formed in the top sediment layers during bed consolidation can result in stable open channels in beds of significant yield stress, typically reported in the kPa range [8]. These stable channels present a mechanism for continuous gas transport from high strength consolidated beds.

These mechanisms promoting gas release from both very weak and very strong sediment beds imply that intermediate strength beds, with yield stresses in the 10s and low 100s Pa, have the greatest capacity for gas retention. However, these continuous gas release mechanisms are supplemented by periodic gas release mechanisms in sediments with high voidages. *Full rollover* occurs when the retained gas reduces the bulk density of the bed below that of the supernatant layer and this *density inversion* drives Rayleigh-Taylor instabilities. *Partial rollover* occurs when a small, high voidage region of the bed becomes buoyant with respect to the surrounding sediment and breaks free of the cohesive and adhesive forces integrating it with the bed. Since the MSSS and Hanford Tanks are continuously ventilated, full rollover is a prerequisite for a spike in hydrogen concentration in the ullage.

METHODS

The brucite, $Mg(OH)_2$, test material used in this study is H3 Versamag (Martin Marietta Magnesia Specialties LLC, USA), a fine white precipitated powder with a specification of less than 1.2 % oxide impurities, a density of 2360 kg m^{-3} and a median particle size of 1.09 µm. Soft sediments were prepared by the addition of tap water prior to 10 minutes of agitation with a pitched blade impeller controlled by an overhead stirrer.

Shear yield stress characterisation

A 4-blade vane attached to a Brookfield DV-II+ Pro Viscometer (Brookfield Engineering Laboratories, USA) was submerged in a 500 ml, 75 mm diameter beaker of magnesium hydroxide soft sediment, such that the top of the vane aligned with the top of the sample. The vane was rotated at a constant speed of 0.5 rpm (0.05 rad s^{-1}) and the drag imposed on the vane by the sample deflects a spring within the Viscometer. This spring deflection is translated to a torque, T, signal by a rotary transducer. The material is said to yield at the maximum in the torque-time profile and this maximum torque, T_{max}, can be translated to a yield stress using the diameter, D, and height, H, of the vane according to Eq. (5), which is modified from Dzuy and Boger [11] as only one end of the vane is in contact with, and hence shears, the sample:

$$\boldsymbol{T_{max} = \frac{\pi D^3}{2}\left(\frac{H}{D} + \frac{1}{6}\right)\tau} \tag{5}$$

A 10.8 mm diameter vane was used for samples of less than 40 % w/w solids concentration. A smaller 6.3 mm diameter vane was required at greater concentrations as the viscometer's maximum torque of 5.75×10^{-3} N m^{-1} limits measurements with the larger vane to stresses of less than 166 Pa.

Laboratory scale gas retention tests

The experimental design for a series of laboratory scale gas retention tests is shown in Figure 1. A 1 l volume of magnesium hydroxide soft sediment was prepared at solids concentrations between 28 and 45 % w/w. A peristaltic pump was used to transfer around 75 % of the test material to an air tight, lidded test cylinder with a diameter of 118 mm. During this transfer a 4 ml volume of 35 % w/w hydrogen peroxide (Merck Chemicals, Germany) was injected into the flow. This hydrogen peroxide decomposes to a 500±60 ml volume of oxygen over the course of 6-14 hrs, depending on light, temperature and pressure conditions, according to Eq. (6):

$$\boldsymbol{H_2O_2 \rightarrow H_2O + \frac{1}{2}O_2} \tag{6}$$

As the hydrogen peroxide decomposes a portion of gas is retained, causing the bed to swell, while the remaining volume escapes to the ullage of the test cylinder. Flexible tubing transports gas from the test cylinder ullage to an upturned measuring cylinder suspended in a water bath. The volume displaced from the upturned cylinder represents the total volume of gas generated by the decomposing hydrogen peroxide at an instant in time, $V_G(t)$. The volume of gas retained by the bed, $V_R(t)$, is estimated from the net increase in bed height in the test cylinder, while the volume of gas which escapes from the bed, $V_E(t)$, can be deduced from the difference between the generated and retained gas volumes.

$$\boldsymbol{V_G(t) = V_R(t) + V_E(t)} \tag{7}$$

The instantaneous void fraction, $v(t)$, of the bed is determined using the ratio of the instantaneous bed height to the initial, gas free, bed height as indicated by Eq. (8). It should be noted that any gas retained by the bed prior to the first measurement is not captured in this void fraction calculation and so *v(t)* represents an increase in void fraction from commencement of the experiment rather than a true absolute void fraction.

$$\boldsymbol{v(t) = 1 - \frac{H_0}{H(t)}} \tag{8}$$

These tests were undertaken without a supernatant layer above the bed as exchange of water between the supernatant and bed, combined with buoyant transfer of solids from the bed, introduces uncertainty regarding the composition of the bed over the course of the experiment and greatly complicates calculation of the void fraction.

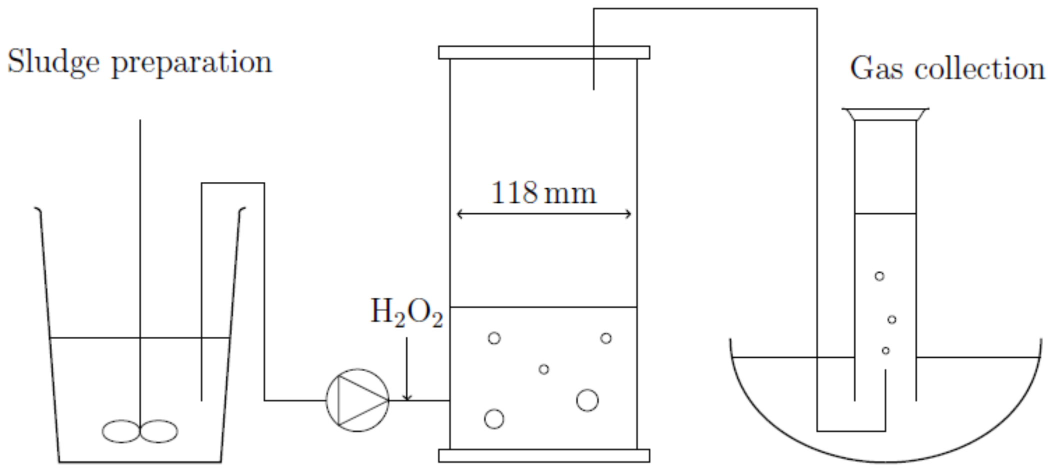

Figure 1: Experimental set-up for gas retention in magnesium hydroxide soft sediments at laboratory scale.

X-ray computed tomography

A Brivo CT385 medical x-ray computed tomography (CT) scanner (GE Healthcare, UK) at the University of Leeds was used to visualize bubbles in 30 % w/w, 7 Pa yield stress, magnesium hydroxide soft sediment. A bespoke test vessel was manufactured from a 290 mm diameter, 150 mm long, side mounted acrylic cylinder. A 6.5 l volume of test material was pumped to the test cylinder using a peristaltic pump and 26 ml hydrogen peroxide was injected into the flow. Cross-sectional images, or *slices*, were captured within a circular *x-y* plane at regular intervals along the length, or *z*-axis, of the side mounted cylinder.

Images were captured for a 96 mm field of view just below the initial surface of the bed at the maximum pixel resolution (*x-y* axis) of 250 µm and a 625 µm separation between slices (*z*-axis). Images were also captured of almost the entire rig in order to capture all large artefacts within the bed. The parameters used for the two types of scan are summarized in Table 1:

Table 1: CT scan parameters used for two alternative fields of view

	Small field of view	Large field of view

X-ray voltage (kVp)	120	120
X-ray tube current (mA)	79	40
Field of view diameter (mm)	96	250
Field of view depth (mm)	20	140
Pixel dimensions (µm)	250	488
Slice separation (µm)	625	1250

ImageJ software was used to undertake three dimensional reconstructions of the CT slices for visualization and perform quantitative analysis of the retained bubble population. For this statistical analysis, bubbles were first distinguished from the bulk sediment through bi-level thresholding of the radiodensity histogram using the widely used Renyi entropy algorithm [13]. The Bolte and Codelières [14] approach was then used to identify interconnected voxels as part of the same bubble and assign each distinct bubble a unique label. The number of voxels in each bubble and voxel dimensions then reveal the volume distribution of the digitized bubbles. Bubbles containing fewer than five voxels were excluded from the statistical analysis.

RESULTS & DISCUSSION

Shear yield stress characterisation

Shear yield stress measurements for magnesium hydroxide sediments are shown in Figure 2. A power law model with solids concentration fits the data with an exponent of 8.55 and a coefficient of determination, R^2, of 0.96. Most of the variation in the data is associated with the values acquired at concentrations above 40 % w/w solids using the smaller of the two vanes. The uncertainty in yield stress measurements using the vane is inversely proportional to the size of the sheared area, while it also becomes more difficult to generate a homogeneous sample at these elevated solids concentrations. Furthermore, Figure 2 demonstrates that this region of greatest uncertainty in the measurements coincides with a very sharp increase in yield stress as a function of solids concentration.

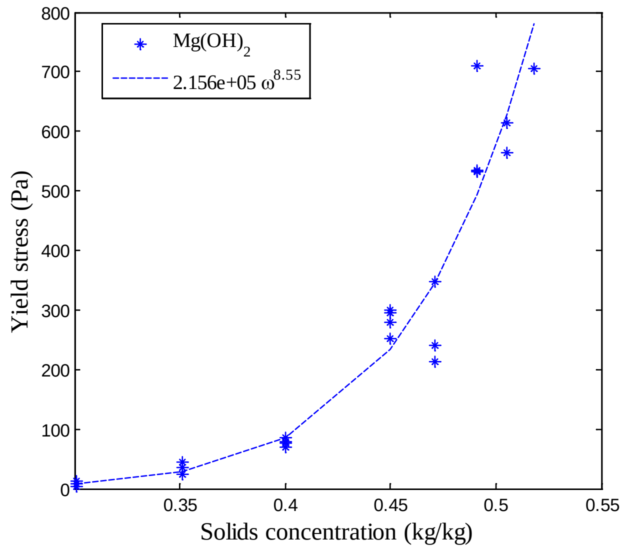

Figure 2: Yield stress measurements for magnesium hydroxide soft sediments using the vane method.

Laboratory scale gas retention tests

Hydrogen peroxide decomposition in the bed resulted in the gas generation profiles shown in Figure 3. Gas is typically generated over the course of 14 hrs, with an exponential decay in the gas generation rate. Good repeatability is largely demonstrated between tests across a broad sediment concentration range. Elevated gas generation rates observed in the 30 and 45 % w/w tests, with gas generation complete within 6 hrs, are associated with experiments which were conducted during the day while the remainder were undertaken through the night. The total volume of generated gas is sensitive to ambient temperature and pressure conditions as well as any uncertainty in the injected hydrogen peroxide volume as 1 ml H_2O_2 decomposes to around 125 ml O_2. The reduced ambient temperature during the night experiments could explain the slower gas generation rates, although reduced *photodegradation* in the absence of sunlight may also contribute. Any sensitivity of the gas generation rate to the concentration of sediment in the bed appeared to be negligible.

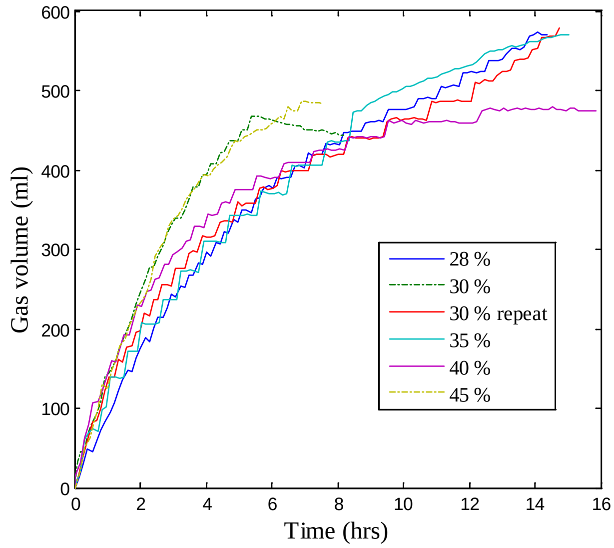

Figure 3: Gas generation profiles due to hydrogen peroxide degradation in sediment beds of different solids concentrations.

Typical profiles of the retained, released and total generated gas volumes evolving with time are shown for a 35 % w/w concentration bed with a 27 Pa yield stress in Figure 4.

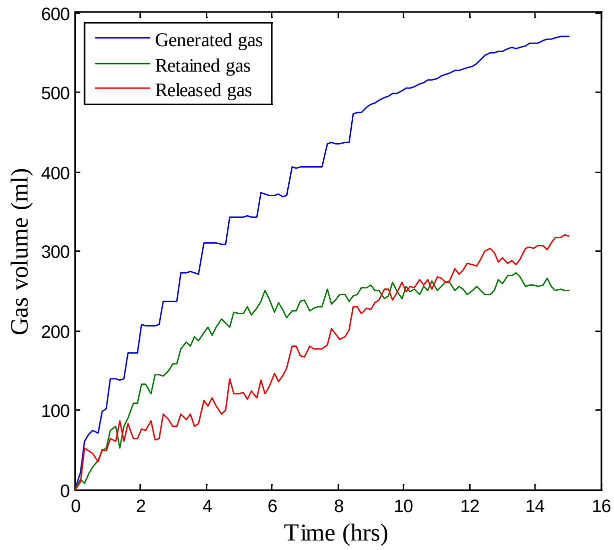

Figure 4: Gas retention and release profiles within a 750 ml bed of 35 % w/w magnesium hydroxide.

The bed swells significantly during the first 4 hrs of gas generation while there is very little further increase in the volume of gas retained by the bed after 6 hrs. A continuous release mechanism allows gas to escape from the bed at a near constant rate of 18 ml hr^{-1}.

From these gas retention profiles, the maximum void fraction was determined across a broad range of yield stress conditions, shown in Figure 5. The largest void factions of 0.27-0.28 were observed in relatively low strength sediment conditions of 7-27 Pa.

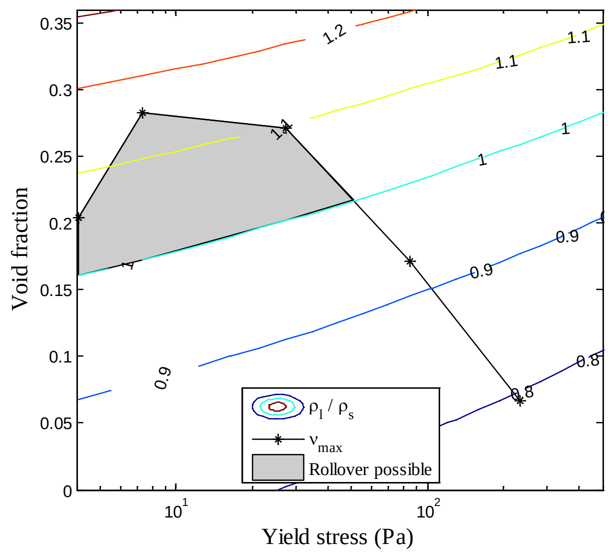

Figure 5: Phase diagram indicating the yield stress conditions required for sufficient gas retention for the bed to achieve buoyancy.

Gas retention by weaker sediment of just 4 Pa yield stress was limited to a void fraction of 0.20. This is explained by the small critical diameter required before bubbles can fluidize the bed, suggesting that bubbles are retained only on short timescales before they grow to a buoyant volume. For beds of 85 and 233 Pa yield stress the capacity for gas retention was substantially reduced, with void fractions of 0.17 and 0.07 respectively. The parabolic dependence of the maximum yield stress with shear yield stress, indicating a reduced capacity for gas retention in low and high strength sediments, is consistent with observations using bentonite clay test materials [15]. However, maximum gas retention in magnesium hydroxide is observed at 7 Pa yield stress as opposed to 30 Pa yield stress in Bentonite clay. Furthermore, the sediment strength conditions in this study are substantially weaker than the kPa yield stress kaolin sediments where the *stable channel* mechanism for gas release has previously been observed [8].

Bentonite clay test materials used by the Pacific Northwest National Laboratory to represent DST waste at Hanford [15], have much greater yield stresses than magnesium hydroxide at equivalent mineral concentrations. Conversely, kaolin test materials favored in marine science studies [8] has lower yield stresses at equivalent concentrations. Either, the microstructure and inter-aggregate bonding within magnesium hydroxide sediments promotes stable channel formation in lower strength sediments, of less than 100 Pa, or a new mechanism for continuous gas release is responsible for the unexpectedly low void fractions observed at 85-233 Pa yield stress. X-ray CT examinations of 85 and 233 Pa sediments, similar to the images of 7 Pa sediment shown in Figure 6, are planned in order to reveal potential mechanisms for gas transport from intermediate strength beds.

Figure 5 presents the maximum void fraction data in conjunction with a contour map of the bulk sediment density, $\rho(\omega,\nu)$, across a range of sediment concentrations and void fractions. The bulk sediment density at a particular void fraction is calculated using Eq. (9), assuming the gas density is much lower than the densities of magnesium hydroxide and water.

$$\boldsymbol{\rho}(\boldsymbol{\omega},\boldsymbol{\nu}) = (\mathbf{1}-\boldsymbol{\nu})\boldsymbol{\rho}_{\boldsymbol{s}} = \frac{\mathbf{1}-\boldsymbol{\nu}}{\frac{\boldsymbol{\omega}}{\rho_{Mg(OH)_2}}+\frac{\mathbf{1}-\boldsymbol{\omega}}{\rho_{H_2O}}} \tag{9}$$

A ratio of supernatant density to bulk sediment density (or inverse specific gravity) in excess of unity indicates a regime where density inversion occurs. The grey area of Figure 5 demonstrates a range of yield stress conditions between 4 and 51 Pa where magnesium hydroxide soft sediments are capable of sufficient gas retention for full rollover to be feasible. Nevertheless, while total rollover may be feasible in this regime, it is far from inevitable. It is more likely that in the presence of supernatant, partial rollover events could transport material to the top of the supernatant and form a *foamy crust*, consistent with observations in Hanford double shell tank waste [16]. Partial rollover events transporting gas to a crust layer could prevent the bed attaining a sufficient voidage to enable full rollover.

The first of many planned x-ray tomography studies was conducted in a 30 % w/w solid concentration, 7 Pa yield stress bed, generating the images shown in Figure 6 which were captured after 6 hrs of gas generation.

After 6 hrs of gas generation, Figure 6 demonstrates that the bed has segregated into a *foam layer*, spanning the top few centimeters of the bed, above the bulk sediment. The foam layer visibly supports a higher voidage, with larger, more irregular bubbles than the bulk sediment. Excluding bubbles less than 5 voxels in volume and those within the foam layer, 1767 bubbles were captured with a volume weighted V_{50} of 4 mm^3. The largest bubble within the bulk sediment was 108 mm^3 in volume, while 90 % of bubbles had a volume less than 43 mm^3. The largest retained bubble within the bed implies that a bubble with a diameter of 5.9 mm is insufficiently buoyant to fluidize the 7 Pa bed.

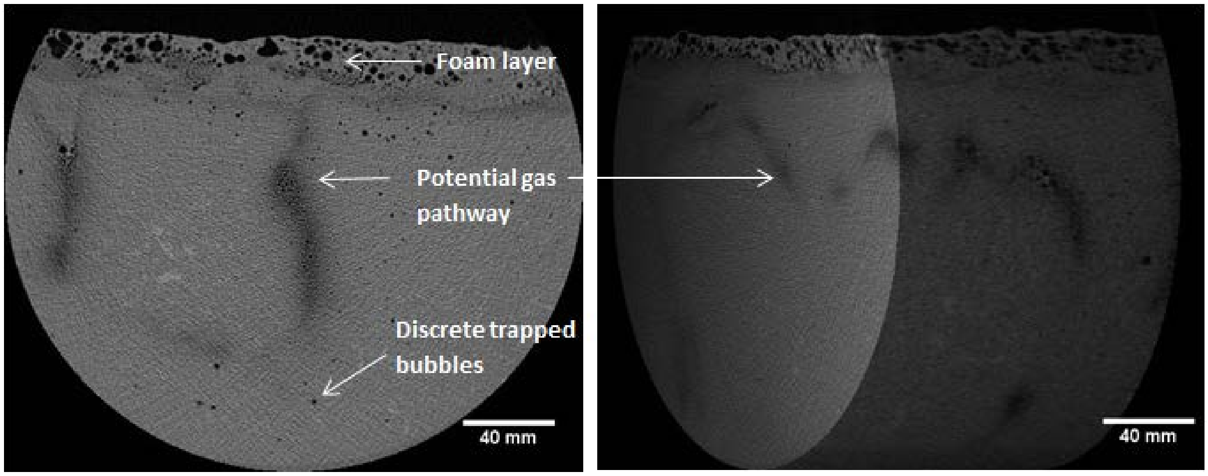

(a) (b)

Figure 6: X-ray computed tomography images in the (a) *x-y* plane and (b) rotated 60° around the *y*-axis, of gas retained in 30 % w/w (7 Pa yield stress) magnesium hydroxide soft sediment.

Another feature of Figure 6 is the dark regions with a high density of microbubbles close to the pixel resolution. These regions could represent a possible avenue for gas transport through the bed and, if these *gas pathways* extend to the vessel walls or the foam layer, could represent an alternative mode of gas release from intermediate strength sediments. Interpolation between the slices along the z-axis in Figure 6(b) confirms that these pathways propagate along the z-y axis as well as through the x-y slice. Introducing the hydrogen peroxide to the soft sediment flow during transport to the test vessel, as shown in Figure 1, could result in inhomogeneous hydrogen peroxide distribution. It is possible that localized gas generation could promote the formation of these gas pathways. Further experiments are planned to investigate whether greater void fractions are observed when gas generation is more homogeneous within the sediment.

CONCLUSIONS

Gas bubbles within soft sediments have been researched by environmental scientists for decades [7-9], however its relevance to legacy nuclear waste in America and the UK is less well reported. Corrosion of first generation, magnox clad, spent fuel during long term underwater storage generates both a cohesive corroded magnox sludge and hydrogen gas. Laboratory scale gas retention tests have revealed a yield stress regime capable of sufficient gas retention for soft sediments to achieve buoyancy with respect to a water supernatant. Interestingly, this regime is observed in much lower strength sediment than the existing mechanisms for gas release discussed in the literature would suggest [8]. X-ray CT images of relatively weak, 7 Pa yield stress sediment reveal a series of regions of high microbubble density, propagating along all three axes. These regions could present pathways for gas transport from the bed.

These channels, submerged beneath the surface of the bed, could represent a distinct gas release mechanism from gas transport through stable open channels reported in van Kessel and van Kesteren [8] and would apply to much weaker sediment of less than 100 Pa yield stress.

REFERENCES

1. G. McCRACKEN and M. EILBECK. Clean up progress on high hazard facilities at Sellafield: magnox swarf storage silos. Proc. ANS Topical Meeting on Decommissioning, Decontamination, and Reutilization, 161–167 (2005).
2. R. BURROWS, S. HARRIS, and N.P.C. STEVENS. Corrosion electrochemistry of fuel element materials in pond storage conditions. *Chemical Engineering Research and Design*, 83 (7A): 887–892, (2005).
3. C.R. GREGSON, D.T. GODDARD, M.J. SARSFIELD, and R.J. TAYLOR. Combined electron microscopy and vibrational spectroscopy study of corroded magnox sludge from a legacy spent nuclear fuel storage pond. *Journal of Nuclear Materials*, 412(1) 145–156, (2011).
4. R.T. ALLEMANN. Physical mechanisms contributing to the episodic gas release from Hanford tank 241-sy-101. *High Level Radioactive Waste Management* 92, Las Vegas, Apr 1992.
5. S. KAM, P.A. GAUGLITZ and W. ROSSEN (2001). Effective compressibility of a bubbly slurry. I. theory of the behaviour of bubbles trapped in porous media. *Journal of Colloid and Interface Science*, 241, 248-259
6. B. BOUDREAU, The physics of bubbles in surficial, soft, cohesive sediments. *Marine and Petroleum Geology*, 38, 1-18 (2012).
7. B.D. JOHNSON, *et al*. Mechanical response of sediments to bubble growth. *Marine Geology* 187.3 347-363 (2002).
8. T. VAN KESSEL & W.G.M. VAN KESTEREN. Gas production and transport in artificial sludge depots. *Waste Management*, 22, 19-28. (2002).
9. O. NAVON, A. CHEKHMIR, and V. LYAKHOVSKY. Bubble growth in highly viscous melts: theory, experiments, and autoexplosivity of dome lavas. *Earth and Planetary Science Letters* 160(3) 763-776. (1998).
10. D. ATAPATTU, R. Chhabra and P. Uhlherr. Creeping sphere motion in Herschel-Bulkley fluids: flow field and drag. *Journal of Non-Newtonian Fluid Mechanics*, 59, 245 (1995)
11. N.Q. DZUY, and D. BOGER, Direct yield stress measurement with the vane method. *Journal of Rheology* 29, 335-347 (1985).
12. P.A. GAUGLITZ, J.R. BONTHA, R.C. DANIEL, L.A. MAHONEY, S.D. RASSAT, B.E. WELLS, J. BAO, G.K. BOERINGA, W.C. BUCHMILLER, C.A. BURNS, J. CHUN, N.K. KARRI, H. LI, AND D.N. TRAN. 2015. Hydrogen Gas Retention and Release from WTP Vessels: Summary of Preliminary Studies. PNNL-24255, *Pacific Northwest National Laboratory, Richland, WA, US* (2015)
13. J.N. KAPUR, P.K. SAHOO, and A.C.K. WONG. A new method for gray-level picture thresholding using the entropy of the histogram. *Graphical Models and Image Processing* 29 (3): 273-285. (1985)
14. S. BOLTE and F.P. CORDELIÈRES. A guided tour into subcellular colocalization analysis in light microscopy. *Journal of Microscopy* 224 (3): 213-232 (2006)

15. P.A. GAUGLITZ, W.C. BUCHMILLER, S.G. PROBERT, A.T. OWEN, and F.J. BROCKMAN. Strong-Sludge Gas Retention and Release Mechanisms in Clay Simulants. PNNL-21167. *Pacific Northwest National Laboratory, Richland, WA, US* (2012).
16. S. BRYAN, L. PEDERSON, and R. SCHEELE. Crust growth and gas retention in synthetic Hanford waste. Proc. Waste Management 92, Tuscon. (1992)

ACKNOWLEDGEMENTS

The authors wish to thank the Engineering & Physical Sciences Research Council (EPSRC) and the National Decommissioning Authority (NDA) for sponsorship funding through an Industrial CASE award. Thanks are also given to Sellafield Ltd. for further funding of research (through the Sludge Centre of Expertise) and in particular Geoff Randall and Martyn Barnes for their support. The authors also wish to thank the Royal Society of Chemistry for their financial support through the SCI-RSC Rideal Travel Bursary. Thanks also to Samuel Allshorn and Carlos Grattoni for their x-ray tomography expertise and to Tony Windross for engineering the test rigs used in this study.